Supplemental Information (SI) for: "Interferometric synthetic aperture radar (InSAR) phase data assimilation for Bayesian snow water equivalent estimation"

Steven A. Margulis[1], Maya Hildebrand[1], Xiaolan Xu[2], Manuela Girotto[3], Hans-Peter Marshall[4], Rashmi Shah[2], Elias Deeb[5], Simon Yueh[2], Dara Entekhabi[6], Jessica Lundquist[7]

[1]Department of Civil & Environmental Engineering, University of California, Los Angeles, 90095, USA
[2]Jet Propulsion Laboratory, California Institute of Technology, Pasadena, 91109, USA
[3]Department of Environmental Science, Policy & Management, University of California, Berkeley, 94720, USA
[4]Department of Geosciences, Boise State University, Boise, 83725, USA
[5]Cold Regions Research and Engineering Laboratory, U.S. Army Corps of Engineers, Hanover, 03755, USA
[6]Department of Civil & Environmental Engineering, Massachusetts Institute of Technology, Cambridge, 02139, USA
[7]Department of Civil & Environmental Engineering, University of Washington, Seattle, 98195, USA

Text S1 Modeling the dielectric properties of snow

The complex permittivity (dielectric constant) of snow is given by:

$$\varepsilon_{snow} = \varepsilon'_{snow} + i\varepsilon''_{snow} \qquad \text{(S1)}$$

where the first term is the real part that characterizes the refraction between air and snow and the reduced wave speed that causes the phase delay (Section 2.2.2). The imaginary part of the snow permittivity (second term in Eq. (S1)) characterizes the attenuation (via absorption) of the signal propagating through snow, which is small for dry snow and much larger for wet snow.

The real part of the permittivity of dry snow is independent of wavelength between 10 MHz and 100 GHz (Johari, 1976; Warren, 1984; Bohleber et al., 2012; Warren and Brandt, 2008), but depends on snow density (ρ_{snow}; Wiesmann and Mätzler, 1999; Proksch et al., 2015). The imaginary part of the dry snow permittivity (Section S1.1; Tiuri et al., 1984) varies between approximately 10^{-5} – 10^{-3}, which represents a small attenuation for dry snow compared to wet snow. For wet snow the complex permittivity depends additionally on the snow volumetric liquid water content (LWC) and the permittivity of liquid water (Section S1.2; Wiesmann and Mätzler, 1999; Proksch et al., 2015).

S1.1 Dry snow

The real part of the permittivity of dry snow can be estimated by (Wiesmann and Mätzler, 1999; Proksch et al., 2015):

$$\varepsilon'_{snow,dry} = \begin{cases} 1 + 1.46674(v) + 1.435(v)^3, & \rho_{snow} \leq 400\ \mathrm{kg/m^3} \\ [0.99913(1-v) + 1.4759(v)]^3, & \rho_{snow} > 400\ \mathrm{kg/m^3} \end{cases} \quad \text{(S2)}$$

where $v = \rho_{snow}/\rho_{ice}$ represents the ice fraction in the snowpack (with the density of ice (ρ_{ice}) equal to 917 kg/m^3). For typical seasonal snowpack densities (i.e., ρ_{snow} between ~100-500 kg/m^3), $\varepsilon'_{snow,dry}$ varies over the range ~1.2 – 2 (Leinss et al., 2015). The lack of frequency dependence of $\varepsilon'_{snow,dry}$ implies that refraction and wave speed reduction through dry snow will behave similarly across wavelength (i.e., for C-, L-, and P-band).

The imaginary part of the dry snow permittivity can be estimated by (Tiuri et al., 1984):

$$\varepsilon''_{snow,dry} = [0.48(v) + 0.52(v)^2]\varepsilon''_{ice} \quad \text{(S3)}$$

where the complex permittivity of ice (ε''_{ice}) is a function of frequency and temperature (Wiesmann and Mätzler, 1999; Proksch et al., 2015). At frequencies between C- through P-band, $\varepsilon''_{snow,dry}$ varies between ~10^{-5} – 10^{-3}. This represents a small attenuation for dry snow compared to wet snow (Sect. S1.2).

S1.1 Wet snow

For wet snow the complex permittivity can be estimated using a Maxwell Garnett mixing model (Wiesmann and Mätzler, 1999; Proksch et al., 2015):

$$\varepsilon_{snow,wet} = \varepsilon'_{snow,wet} + i\varepsilon''_{snow,wet} = \frac{(1-LWC)\varepsilon_{snow,dry} + (LWC)\varepsilon_{water}K}{1 - LWC + (LWC)K} \quad \text{(S4)}$$

where ε_{water} ($\varepsilon'_{water} + i\varepsilon''_{water}$) is the complex permittivity of liquid water (and is a function of temperature and frequency, Liebe et al., 1991), and

$$K = \frac{1}{3}\sum_{k=1}^{3} \frac{\varepsilon_{snow,dry}}{\varepsilon_{snow,dry} + A_k(\varepsilon_{water} - \varepsilon_{snow,dry})} \quad \text{(S5)}$$

with depolarization factors: $A_1 = 0.005, A_2 = A_3 = 0.4975$. At LWC=0%, Eq. (S4) reduces to the dry snow permittivity. The imaginary part of $\varepsilon_{snow,wet}$ comes primarily through ε''_{water}.

In Eq. (S4), variations in $\varepsilon''_{snow,wet}$ are primarily dictated by LWC variations rather than snow density variations. Figure S1 illustrates $\varepsilon''_{snow,wet}$ as a function of LWC at C-, L-, and P-bands. Snow wetness significantly increases $\varepsilon''_{snow,wet}$ by many orders of magnitude over dry snow. As LWC or frequency increases, $\varepsilon''_{snow,wet}$ increases (implying more absorption).

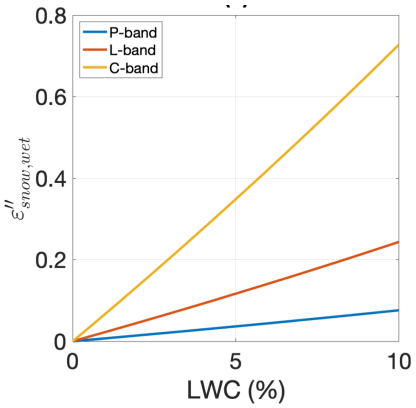

Figure S1. Imaginary part of permittivity of wet snow at C-, L-, and P-band frequencies.

Text S2 Multi-layer, multiple reflection model for phase delay

To fully account for absorption and multiple reflections at the (i) air-snow interface, (ii) snow-soil interface, and (iii) any other internal snowpack layers (i.e., with varying LWC or other snow properties), the reflection coefficient for the bulk snowpack can be computed using a layered dielectric medium model as illustrated in Yueh et al. (2017; their Fig. 16). For a layered medium with d_l being the height of an interface with $l = 0$ (air-snow interface) , … , n (snow-soil interface), and layers in between characterized by their respective dielectric properties, a recurrence relation can be derived by matching boundary conditions of the electric fields at each interface. For example, at horizontal polarization (Tsang et al., 1985: p. 26-28 and Ulaby and Long, 2014: p. 67)):

$$(AB)_l e^{-i2k_{lz}d_l} = \frac{(AB)_{l+1} e^{-i2k_{(l+1)z}d_{l+1}} e^{-i2k_{(l+1)z}(d_{l+1}-d_l)} + R_{l(l+1)}}{(AB)_{l+1} e^{-i2k_{(l+1)z}d_{l+1}} R_{l(l+1)} e^{-i2k_{(l+1)z}(d_{l+1}-d_l)} + 1} \qquad \text{(S6)}$$

where $(AB)_l$ is the ratio of amplitudes of the downwelling and upwelling electric fields respectively, $k_{lz} = \sqrt{k_0^2 \varepsilon_l - (k_0 \sin\ \theta_T)^2)}$, k_0 is the wavenumber ($2\pi/\lambda$), ε_l is the permittivity of layer l, and $R_{l(l+1)}$ is the reflection coefficient at the interface between layers l and $l+1$, which is given by:

$$R_{l(l+1)} = \frac{\mu_{l+1} k_{lz} - \mu_l k_{(l+1)z}}{\mu_{l+1} k_{lz} + \mu_l k_{(l+1)z}} \qquad \text{(S7)}$$

In this formulation, the air at the top interface and soil at the bottom interface are treated as semi-infinite half spaces. Once the recursion is applied from the snow-soil interface to the air-snow interface, the reflection coefficient at the air-snow interface is given by: $R_0 = (AB)_0$. A similar formulation can be applied for vertical polarization, which could be combined to get the

reflection coefficient for circular polarization. Finally, the phase delay can be computed as the angle of the complex reflection coefficient (at the air-snow interface) relative to a reference case (i.e., a previous snow state):

$$\phi_{snow} = \angle(R_0)_{t_{m2}} - \angle(R_0)_{t_{m1}} \qquad \text{(S8)}$$

where the 0 subscript denotes the air-snow interface and t_{m1} and t_{m2} are two measurement times. This layered model is difficult to apply in retrieval approaches due to the lack of information on layering, but in the context of data assimilation can be useful if the snow model provides a multi-layer representation of the snowpack. In the context of this study, which uses the FSM2 snow model, the number of layers will vary between one and three layers. The layered model for dry-snow is closely approximated by the first-order approximation of Eq. (2) as shown in Fig. S2a.

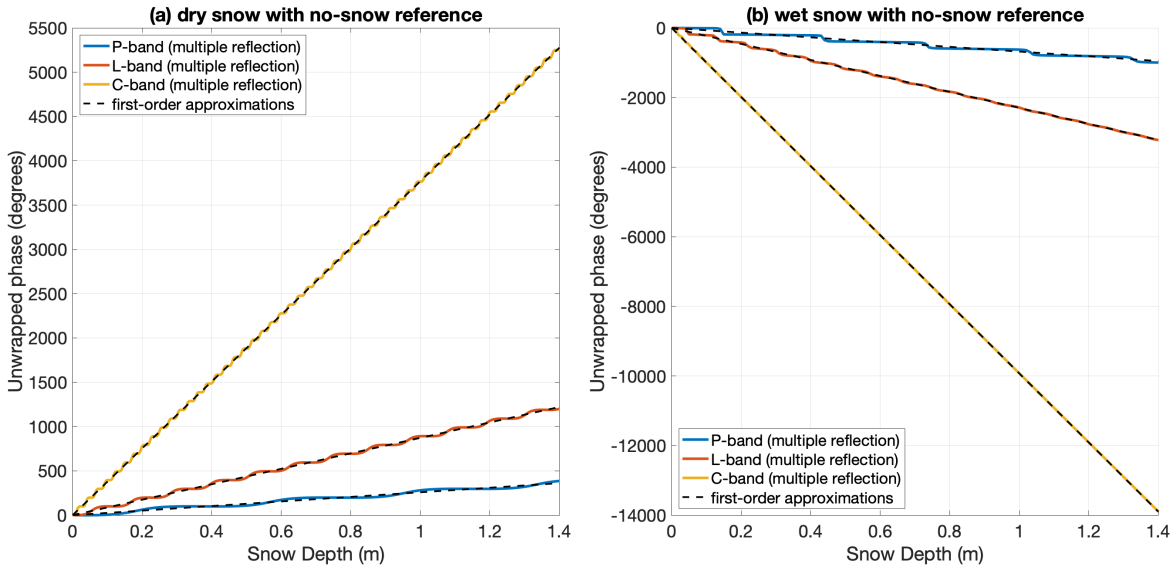

Figure S2. (a) Dry-snow unwrapped phase delay for C-, L-, and P-band as a function of snow depth using a multiple reflection model (colored lines) and the first-order approximation given by Eq. (2) with $\boldsymbol{I} = \mathbf{1}$ (dashed lines). (b) Wet-snow (with LWC value of 3%) unwrapped phase delay C-, L-, and P-band as a function of snow depth using a multiple reflection model and the first-order approximation for wet snow given by Eq. (2) with $\boldsymbol{I} = \mathbf{0}$ or equivalently Eq. S9 (dashed lines). Both cases are shown relative to a no-snow reference for ease of visualization.

For sufficiently wet snow, the air-snow interface will provide the dominant reflection source (Fig. S3). Layering is often more important in wet snow, since LWC can be large near the snowpack surface where snowmelt originates and LWC can be near-zero lower in the snowpack until the snowpack becomes isothermal and/or water drains to lower layers. Hence, using a depth-averaged (equivalent single layer snowpack) LWC may erroneously predict the phase delay behavior since LWC values in surface layers may be sufficiently large to limit penetration of the signal, while depth-averaged values (where the snowpack is dry in lower layers) may underestimate that effect. As in the dry-snow case, the layered multiple reflection model

(Eq. (S8)) can be used to determine the phase from the computed reflection coefficient (with LWC profile as an additional input). Alternatively, the first-order approximation for phase delay between two measurement times in sufficiently wet snow conditions is given by (Yueh et al., 2017):

$$\phi_{snow} = -2k_0 \Delta d_{snow} \cos(\theta_T) \qquad \text{(S9)}$$

which is equivalent to Eq. (2) with with $\boldsymbol{I} = 0$ and where there is only dependence on snow depth changes (and not snow density). Thus, in the case of sufficiently wet snow, the phase delay will decrease with increasing SWE ($\partial\phi_{snow}/\partial SWE < 0$) since the snow surface (dominant reflection source) is closer to the receiver. Figure S2b shows the phase delay in wet snow conditions (LWC = 3%) for a simple single-layer snowpack. Under these "sufficiently wet" conditions, the phase delay becomes negative, indicating the snowpack reflection behaves schematically as shown in Fig. S3 and is well approximated by Eq. (S9). Note that there is a frequency-dependent snow-wetness induced transition (not shown) between behavior described by Eq. (2) and Eq. (S9). It is in this transition (i.e., typically between LWC = 0-3%) that phase delay cannot be approximated by the first-order approximations of Eq. (2) or (S9) such that it is expected that under those conditions no phase information would be retrievable.

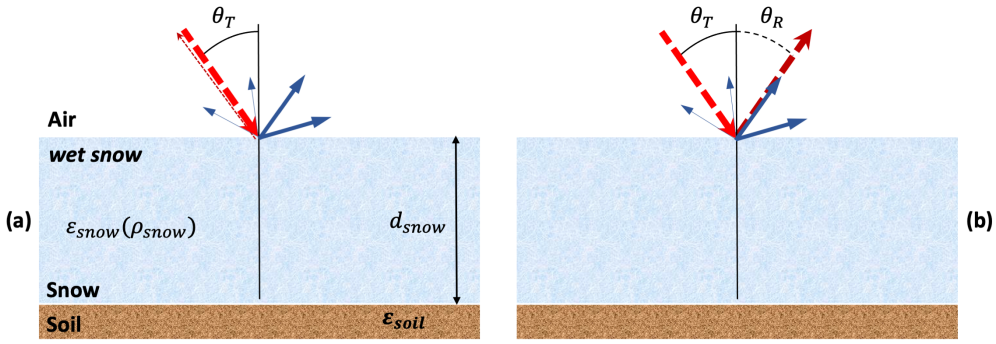

Figure S3. Illustration of first-order scattering for sufficiently wet snow with (a) monostatic (backscattering) and (b) bistatic (forward scattering) cases respectively.

Text S3 Sources of error in measured phase

Beyond phase delay associated with snow, other factors contribute to phase changes between a pair of measurements. The total measured phase change (ϕ_{meas}) is the superposition of phase changes from other sources (Wu and Madson, 2024; Hoppinen et al., 2025), e.g.:

$$\phi_{meas} = \phi_{topo} + \phi_{orbit} + \phi_{atmos} + \phi_{deform} + \phi_{veg} + \phi_{soil} + \phi_{snow} + \phi_{noise} \quad \text{(S10)}$$

where ϕ_{topo} is related to topographic effects, ϕ_{orbit} is related to changes in transmitter-receiver orbital position/s, ϕ_{atmos} is related to changes in signal propagation through the atmosphere (due to tropospheric water content and ionospheric total electron content), ϕ_{deform} is related to terrain deformation, ϕ_{veg} is related to changes in surface vegetation, ϕ_{soil} is related to changes in soil moisture, and ϕ_{noise} represents random changes typically associated with decorrelation between measurement pairs and/or instrument noise. Equation (S10) can be used to estimate the phase delay associated with snow changes where the mean is given by:

$$\phi_{snow,obs} = \phi_{meas} - \bar{\phi}_{topo} - \bar{\phi}_{orbit} - \bar{\phi}_{atmos} - \bar{\phi}_{deform} - \bar{\phi}_{veg} - \bar{\phi}_{soil} - \bar{\phi}_{noise} \quad \text{(S11)}$$

which allows for correcting the measured phase change (ϕ_{meas}) by any non-snow terms that have non-zero (systematic) mean phase differences between measurements. In retrieval algorithms, $\phi_{snow,obs}$ from Eq. (S11) is used deterministically to invert Eq. (2) to estimate SWE changes. In the Bayesian data assimilation approach proposed in this paper, the snow phase delay uncertainty is also a key parameter dictating how uncertain the assimilated measurement is. Assuming the terms in Eq. (S11) are independent, the uncertainty in ϕ_{snow} can be estimated as:

$$(\sigma_{\phi_{snow}})^2 = (\sigma_{\phi_{topo}})^2 + (\sigma_{\phi_{orbit}})^2 + (\sigma_{\phi_{atmos}})^2 + (\sigma_{\phi_{deform}})^2 + (\sigma_{\phi_{veg}})^2 + (\sigma_{\phi_{soil}})^2 + (\sigma_{noise})^2 \quad \text{(S12)}$$

where the terms on the right-hand-side represent uncertainties in each of the contributing terms to phase changes (Hoppinen et al., 2025). In practice, the measurement uncertainty ($\sigma_{\phi_{snow}}$) in phase retrieval is expected to vary in space-time and with frequency based on the specific terms in Eq. (S10). In applications with real data, the Bayesian measurement model could include Eqs. (S11) and (S12) to characterize $\phi_{snow,obs}$ and $\sigma_{\phi_{snow}}$. Herein, we don't apply these equations, but for simplicity use unbiased $\phi_{snow,obs}$ (i.e. the case where non-snow terms of been successfully removed) and use a bulk value for the measurement error standard deviation $\sigma_{\phi_{snow}}$.

Text S4 Temporal decorrelation

Temporal decorrelation between pairs of measurements can additionally limit the use of interferometry for deriving phase changes for SWE estimation. The key snow factors that are expected to cause decorrelation at C- through P-band are sub-pixel spatial variations between measurement scenes of: (i) snow depth (or SWE) due to nonuniform snow accumulation and ablation and/or (ii) liquid water content in the snowpack (Rott et al., 2003). Based on an assumed sub-grid distribution describing between-scene variations in snow depth, Rott et al. (2003) quantified the frequency effects on the expected temporal correlation. Figure S4a shows the relationship for P-, L-, and C-band. There is a strong wavelength dependence conditional on sub-grid variations that may arise between measurements. P-band is most robust to between-scene sub-grid variations with

temporal correlation of > 0.9 for up to 100 mm sub-grid snow depth variations. For a temporal correlation > 0.6, C- and L-band measurement footprints should have sub-pixel snow depth variations of less than ~15 mm and ~70 mm respectively between two measurements, which is expected to be restrictive. The practical implication of this is that for a given repeat-frequency, fewer pairs of dry-snow measurements with sufficient correlation needed to derive phase differences would be available at C-band compared to L- and P-band.

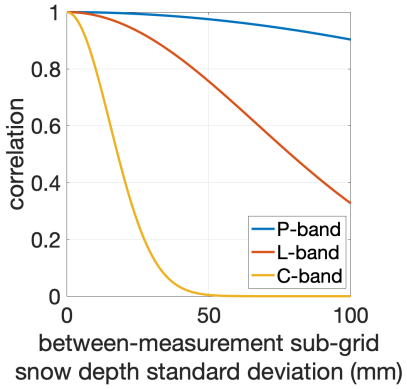

Figure S4. Temporal correlation as a function of dry-snow sub-grid snow depth variation changes between two scenes (adapted from Rott et al., 2003). Values shown are for a snow density of 300 kg m^{-3} and highlight the expected relative temporal decorrelation as a function of frequency.

Text S5 Wrapped phase

Figure S5 shows the wrapped phase delay for dry snow (relative to a no-snow reference) as a function of snow density, snow depth, and frequency. Lower frequencies span more SWE per wrapping cycle. The implication is that for a given SWE change, there is a higher probability of phase ambiguity due to wrapping at C-band than at P-band.

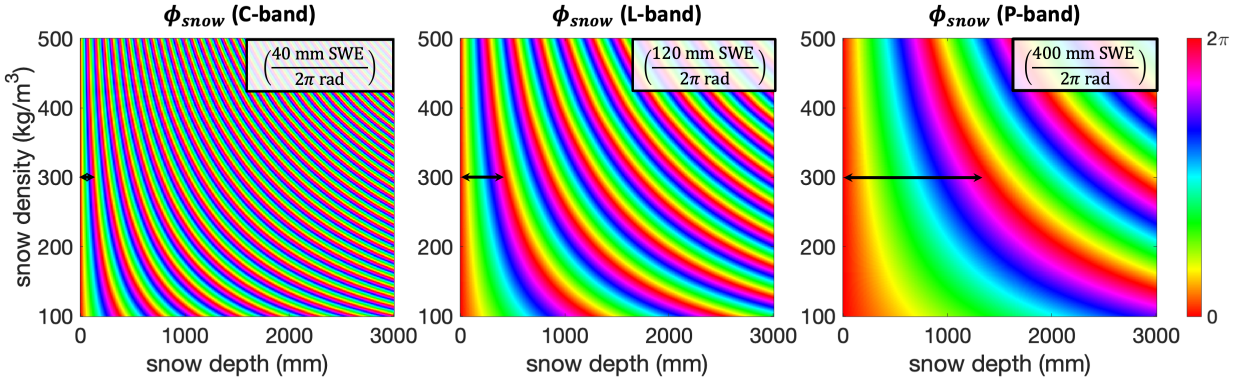

Figure S5. Dry snow (wrapped) phase delay from Eq. (2) over a range of typical seasonal snow densities and depths for C-band (left panel), L-band (middle panel) and P-band (right panel). The black arrow shows the snow depth change over one 2π fringe at a snow density of 300 kg/m^3. While depth changes associated with one fringe vary with density, the SWE change is relatively invariant and shown for each frequency in the upper right corner of each panel.

Text S6 FSM2 Model Setup

FSM2 is a modular snow model where in this application physically-based parameterizations were chosen over more empirical options. For snow albedo, the prognostic (age-based) model used by the CLASS (Verseghy, 1991), ISBA (Boone, 2002), and Noah-MP (Niu et al., 2011) models is used. Turbulent surface exchange is modeled with the Richardson number stability correction option (Louis et al., 1991), which is used in several snow models including BATS (Yang et al., 1997), CLASS, Crocus (Vionnet et al., 2012), ISBA, SNTHERM (Jordan, 1991), and others. Of particular importance is the modeling of snow density and LWC, which influence the dielectric properties of snow (Text S1). Snow density evolution is modeled with viscous compaction by overburden and thermal metamorphism based on the original development by Anderson (1976) and since implemented in several snow models including CLM (Oleson et al., 2004), HTESSEL (Dutra et al., 2010), ISBA, SAST (Sun et al., 1999; Xiao et al., 2004), SNTHERM, and VIC (Andreadis et al., 2008). Fresh snow density is modeled empirically as a function of air temperature and windspeed as done in the CLM and Crocus models. The snow LWC evolution is based on a gravitational drainage model used in SNTHERM, which neglects capillary force effects beyond the parameterization of an irreducible (mass fraction) water content (W_{irr}). The FSM2 default value of W_{irr} is 0.03 (as taken from CLM), but different values are used by other models (i.e., ~0.05-0.16 for Crocus, Noah-MP and SNOWPACK). Measurements by Coléou and Lesaffre (1998) indicate values on the order of 0.05-0.15. Based on this range of values, W_{irr} is set to 0.10 in this study.

Text S7 Particle filter with parameter estimation

The version of the particle filter used herein was proposed by Liu and West (2001), which combines estimation of the state vector $\boldsymbol{x_t}$ and a fixed parameter vector β. It provides an alternative to the method of parameter estimation using state augmentation (e.g., Moradkhani et al., 2005) and is designed to mitigate particle ensemble degeneracy. The extension to parameter estimation in this work is chosen so that the key precipitation bias correction parameter b (used in Eq. (6)) is estimated sequentially along with the snow states. Since b is postulated as lognormal, and the Liu and West (2001) method assumes a Gaussian distribution for parameters, we set $\beta = \log(b)$ where β is characterized by its mean $\bar{\beta}_t$ and variance ${\sigma_\beta}_t^2$. The prior values for the mean and coefficient of variation in b described in Section 3.3.3 can be used to estimate the prior parameter values for β.

The particle set consisting of states and parameters at a given time is given by $\{(\boldsymbol{x}_t, \beta_t)^{(i)}\}_{i=1}^{N}$, which is meant to approximate the posterior PDF $p(\boldsymbol{x}_t, \beta_t | y_t)$. At the very beginning of the integration period ($t = 0$), these represent fully prior estimates (each with equal weight ($w_t^{(i)} = 1/N$), whereas otherwise they represent the most recent posterior estimate, which serves as the prior estimate for the next measurement. The sequential particle filter aims to derive the posterior estimate $\{(\boldsymbol{x}_{t+1}, \theta_{t+1})^{(i)}\}_{i=1}^{N}$ at the next measurement time ($t + 1$).

Between measurement times (from t to $t + 1$) there are two propagation and update steps associated with the parameter and state vectors. First, the expected value of the state vector at the measurement time is given by:

$$g\left(\boldsymbol{x}_t{}^{(i)}\right) = E(\boldsymbol{x}_{t+1}|\boldsymbol{x}_t{}^{(i)}, m(\beta_t{}^{(i)})) \quad \text{(S13)}$$

where $m\left(\beta_t{}^{(i)}\right) = a\beta_t{}^{(i)} + (1-a)\bar{\beta}_t$ represents a parameter value estimate using a kernel smoothing approach (Liu and West, 2001), where a is a shrinkage factor (~0.97-0.99). Intermediate posterior weights ($\pi_{t+1}^{(i)}$) on individual particles are derived from the likelihood function, i.e.:

$$\pi_{t+1}^{(i)} \propto p_{y|x}\left(y_{t+1}|g\left(\boldsymbol{x}_t{}^{(i)}\right), m(\beta_t{}^{(i)})\right) \quad \text{(S14)}$$

where y_{t+1} represents the predicted measurement at the new time step and $p_{y|\boldsymbol{x}}$ the likelihood function Eq. (5). The wetness of the snowpack in a particular ensemble member (particle) i dictates whether Eq. (2) or Eq. (S9) is used to predict the phase. Given that the true phase and synthetic measurements are generated for dry-snow only (Fig. 6), this will tend to lead to larger phase errors and therefore reduced weights for wet-snow ensemble members. Based on the calculated weights, the states and parameters are resampled (herein using systematic resampling; Kuptamatee and Aunsri, 2022) to equally weighted values: $\{(\tilde{\boldsymbol{x}}_t, \tilde{\beta}_t)^{(i)}\}_{i=1}^N$. The parameter particles ($\tilde{\beta}_{t+1}^{(i)}$) are updated by sampling from the distribution $N(m(\tilde{\beta}_t{}^{(i)}), h^2\sigma_{\beta_t}{}^2)$, where $h^2 = \sqrt{1-a^2}$. Using the new parameter values, the states are repropagated over the assimilation window to get $\tilde{\boldsymbol{x}}_{t+1}$, and the posterior weights ($w_{t+1}^{(i)}$) are derived via:

$$w_{t+1}^{(i)} \propto \frac{p_{y|x}\left(y_{t+1}|\tilde{\boldsymbol{x}}_{t+1}, \tilde{\beta}_{t+1}^{(i)}\right)}{p_{y|x}\left(y_{t+1}|g(\boldsymbol{x}_t{}^{(i)}), m(\beta_t{}^{(i)})\right)} \quad \text{(S15)}$$

In Eqs. (S14) and (S15) the absolute values of the weights are determined by normalizing the likelihood-based values by their summation across the ensemble so that the weights sum up to 1.0. The final posterior estimate $\{(\boldsymbol{x}_{t+1}, \beta_{t+1})^{(i)}\}_{i=1}^N$ is determined by again systematic resampling using the derived weights so that each particle is then equally weighted ($1/N$) before moving to the next assimilation window.

For the case with unwrapped phase measurements, the likelihood function (Eq. (5)) is the normal (Gaussian) distribution, i.e. (shown for the univariate case used herein):

$$p_{y|\boldsymbol{x}} = p_v = \frac{1}{\sigma_{\phi_{snow}}\sqrt{2\pi}} \exp\left(-\frac{v^2}{2(\sigma_{\phi_{snow}})^2}\right) \quad \text{(S16)}$$

where v is the error in predicted phase (assumed zero-mean) and $\sigma_{\phi_{snow}}$ is the specified phase error standard deviation used to characterize the uncertainty in the derived snow-related phase measurement ($\phi_{snow,obs}$). Note in practice that and $\sigma_{\phi_{snow}}$ may vary in time (i.e., for different measurement pairs) according to Eq. (S12), but is specified as a constant parameter in the experiments performed herein. When considering wrapped phase measurements, the wrapped normal distribution (Agiomyrgiannakis and Stylianou, 2009; Kumar et al., 2022) is a more appropriate model for the phase measurement error and the likelihood function, i.e.:

$$p_{y|x} = p_v = \frac{1}{\sigma_{\phi_{snow}}\sqrt{2\pi}} \sum_{l=-\infty}^{\infty} \exp\left(-\frac{(v-2\pi l)^2}{2(\sigma_{\phi_{snow}})^2}\right) \quad \text{(S17)}$$

An illustrative example of the wrapped normal distribution is shown in Fig. S6. For small measurement error standard deviation, the wrapped normal approaches the normal distribution, while for large measurement error standard deviation it approaches the uniform distribution. The primary consequence of using the wrapped normal distribution is that phase errors that are 2π multiples of each other will have the exact same likelihood.

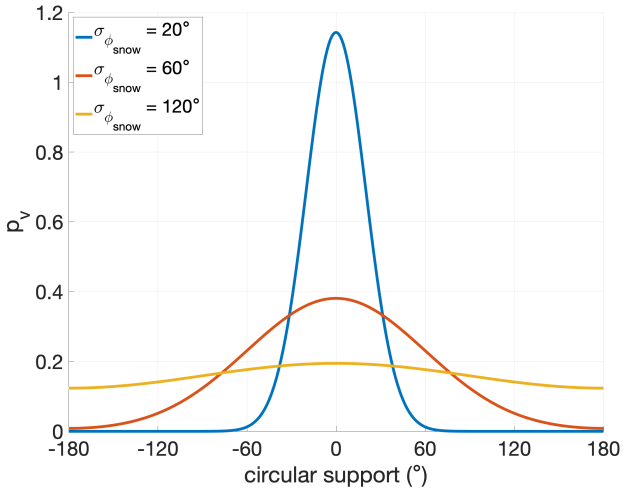

Figure S6. Wrapped normal distribution used for the wrapped phase likelihood function in the particle filter. Each curve corresponds to a different measurement error standard deviation.

References

Agiomyrgiannakis, Y. and Stylianou, Y.: Wrapped Gaussian Mixture Models for Modeling and High-Rate Quantization of Phase Data of Speech. *IEEE Trans. Audio Speech Lang. Process.*, 17(4), 775–786, https://doi.org/10.1109/TASL.2008.2008229, 2009.

Anderson, E. A.: A point energy and mass balance model of a snow cover. NOAA Technical Report NWS 19, Office of Hydrology, National Weather Service, 1976.

Andreadis, K. M., Storck, P., and Lettenmaier, D. P.: Modeling snow accumulation and ablation processes in forested environments. *Water Resour. Res.*, 45, https://doi.org/10.1029/2008WR007042, 2009.

Bohleber, P., Wagner, N., and Eisen, O.: Permittivity of ice at radio frequencies: Part II. Artificial and natural polycrystalline ice. *Cold Reg. Sci. Technol.*, 83–84, 13–19, https://doi.org/10.1016/j.coldregions.2012.06.002, 2012.

Boone, A.: Description du schema de neige ISBA-ES (Explicit Snow). Centre National de Recherches Météorologiques, Météo-France, http://www.cnrm.meteo.fr/IMG/pdf/snowdoc.pdf, 2002.

Coléou, C. and Lesaffre, B.: Irreducible water saturation in snow: experimental results in a cold laboratory. *Ann. Glaciol.*, 26, 64–68, https://doi.org/10.3189/1998AoG26-1-64-68, 1998.

Dutra, E., Balsamo, G., Viterbo, P., Miranda, P. M. A., Beljaars, A., Schär, C., and van den Hurk, B.: An improved snow scheme for the ECMWF land surface model: description and offline validation. *J. Hydrometeorol.*, 11, 899–916, https://doi.org/10.1175/2010JHM1249.1, 2010.

Hoppinen, Z., Palomaki, R. T., Marshall, H.-P., et al.: Separating Snow from Signal: Quantifying Non-Snow Errors in InSAR SWE Retrievals. *TechRxiv*, https://doi.org/10.36227/techrxiv.175433198.81344547/v1, 2025.

Johari, G. P.: The dielectric properties of H2O and D2O ice Ih at MHz frequencies. *J. Chem. Phys.*, 64(10), 3998–4005, https://doi.org/10.1063/1.432655, 1976.

Jordan, R.: A one-dimensional temperature model for a snow cover. Technical documentation for SNTHERM.89. CRREL Special Report 91-16; US Army Corps of Engineers Cold Regions Research and Engineering Laboratory, 1991.

Kumar, G., Date, P., Pachori, R. B., Swaminathan, R., and Singh, A. K.: Wrapped Particle Filtering for Angular Data. *IEEE Access*, 10, 90287–90298, https://doi.org/10.1109/ACCESS.2022.3200478, 2022.

Kuptametee, C., and Aunsri, N.: A review of resampling techniques in particle filtering framework. *Measurement*, 193, https://doi.org/10.1016/j.measurement.2022.110836, 2022.

Leinss, S., Wiesmann, A., Lemmetyinen, J., and Hajnsek, I.: Snow Water Equivalent of Dry Snow Measured by Differential Interferometry. *IEEE J. Sel. Top. Appl. Earth Obs. Remote Sens.*, 8(8), 3773–3790, https://doi.org/10.1109/JSTARS.2015.2432031, 2015.

Liu, J. and West, M.: Combined Parameter and State Estimation in Simulation-Based Filtering, in: Sequential Monte Carlo Methods in Practice, edited by: Doucet, A., de Freitas, N., and Gordon, N., Statistics for Engineering and Information Science, Springer, New York, NY, 197–223, https://doi.org/10.1007/978-1-4757-3437-9_10, 2001.

Liebe, H. J., Hufford, G. A., and Manabe, T.: A Model for the complex permittivity of water at frequencies below 1 GHz. *Int. J. IR Millim. Waves*, 12(7), 659–675, https://doi.org/10.1007/BF01007137, 1991.

Louis, J. F., Tiedtke, M., and Geleyn, J. F.: A short history of the operational PBL-parameterization at ECMWF. Workshop on boundary layer parameterization, ECMWF, http://old.ecmwf.int/publications/library/ecpublications/_pdf/workshop/1981/PBL/ws_pbl_louis.pdf, 1981.

Moradkhani, H., Hsu, K.-L., Gupta, H., and Sorooshian, S.: Uncertainty assessment of hydrologic model states and parameters: Sequential data assimilation using the particle filter, Water Resour. Res., **41**, W05012, https://doi.org/10.1029/2004WR003604, 2005.

Niu, G. Y., Yang, Z. L., Mitchell, K. E., Chen, F., and Wetzel, P. J.: The community Noah land surface model with multiparameterization options (Noah-MP): 1. Model description and evaluation with local-scale measurements. *J. Geophys. Res.*, 116, https://doi.org/10.1029/2010JD015139, 2011.

Oleson, K. W., Dai, Y., Bruland, W., and Lawrence, D. M.: Technical description of the Community Land Model (CLM). NCAR Technical Note NCAR/TN-461+STR; National Center for Atmospheric Research, 2004.

Proksch, M., Mätzler, C., Wiesmann, A., Lemmetyinen, J., Schwank, M., Löwe, H., and Schneebeli, M.: MEMLS3&a: Microwave Emission Model of Layered Snowpacks adapted to include backscattering. *Geosci. Model Dev.*, 8, 2611–2626, https://doi.org/10.5194/gmd-8-2611-2015, 2015.

Rott, H., Nagler, T., and Scheiber, R.: Snow Mass Retrieval by Means of SAR Interferometry. In *FRINGE '03 Workshop: Advances in SAR Interferometry from ERS and ENVISAT Missions*, 1–6, 2003.

Sun, S., Jin, J., and Xue, Y.: A simple snow-atmosphere-soil transfer model. *J. Geophys. Res.*, 104, 19587–19597, https://doi.org/10.1029/1999JD900752, 1999.

Tiuri, M. E., Sihvola, A., Nyfors, E., and Hallikainen, M.: The complex dielectric constant of snow at microwave frequencies. *IEEE J. Oceanic Eng.*, OE-9, 377–382, https://doi.org/10.1109/JOE.1984.1145657, 1984.

Tsang, L., Kong, J. A., and Shin, R. T.: Theory of Microwave Remote Sensing. Wiley Series in Remote Sensing and Image Processing, 1985.

Ulaby, F., and Long, D.: Microwave Radar and Radiometric Remote Sensing (1st ed.). Artech House, 2015.

Verseghy, D. L.: CLASS – a Canadian land-surface scheme for GCMs. I. Soil model. *Int. J. Climatol.*, 11, 111–133, https://doi.org/10.1002/joc.3370110108, 1991.

Vionnet, V., Brun, E., Morin, S., Boone, A., Faroux, S., Le Moigne, P., and Willemet, J. M.: The detailed snowpack scheme Crocus and its implementation in SURFEX v7. *Geosci. Model Dev.*, 5, 773–791, https://doi.org/10.5194/gmd-5-773-2012, 2012.

Warren, S. G.: Optical constants of ice from the ultraviolet to the microwave. *Appl. Opt.*, 23(8), 1206–1225, https://doi.org/10.1364/AO.23.001206, 1984.

Warren, S. G., and Brandt, R. E.: Optical constants of ice from the ultraviolet to the microwave: A revised compilation. *J. Geophys. Res. Atmos.*, 113(D14), 1–10, https://doi.org/10.1029/2007JD009744, 2008.

Wiesmann, A., and Mätzler, C.: Microwave emission model of layered snowpacks. *Remote Sens. Environ.*, 70, 307–316, https://doi.org/10.1016/S0034-4257(99)00108-1, 1999.

Wu, Y.-Y. and Madson, A.: Error Sources of Interferometric Synthetic Aperture Radar Satellites, Remote Sens., **16**, 354, https://doi.org/10.3390/rs16020354, 2024.

Xiao, Z., Sun, S., Jin, J., and Xue, Y.: Development of the Snow-Atmosphere-Soil Transfer model. *J. Appl. Meteorol.*, 43, 888–899, https://doi.org/10.1175/1520-0450(2004)043<0888:DOTSAT>2.0.CO;2, 2004.

Yang, Z.-L., Dickinson, R., Robock, A., and Vinnikov, K.: Validation of the Snow Submodel of the Biosphere–Atmosphere Transfer Scheme with Russian Snow Cover and Meteorological Observational Data, *J. Climate*, **10**, 353–373, https://doi.org/10.1175/1520-0442(1997)010<0353:VOTSSO>2.0.CO;2, 1997.

Yueh, S., Xu, X., Shah, R., Kim, Y., Garrison, J., Komanduru, A., and Elder, K.: Remote Sensing of Snow Water Equivalent Using Coherent Reflection From Satellite Signals of Opportunity: Theoretical Modeling, *IEEE J. Sel. Top. Appl. Earth Obs. Remote Sens.*, 10, 1–12, https://doi.org/10.1109/JSTARS.2017.2743172, 2017.